

See discussions, stats, and author profiles for this publication at: <https://www.researchgate.net/publication/228673397>

# Dynamic Characterization of Graphene Growth and Etching by Oxygen on Ru (0001) by Photoemission Electron Microscopy

ARTICLE *in* THE JOURNAL OF PHYSICAL CHEMISTRY C · NOVEMBER 2009

Impact Factor: 4.77 · DOI: 10.1021/jp907949a

---

CITATIONS

26

READS

2

## 5 AUTHORS, INCLUDING:



**Yi Cui**

Fritz Haber Institute of the Max Planck Soci...

27 PUBLICATIONS 701 CITATIONS

[SEE PROFILE](#)



**Hui Zhang**

Chinese Center For Disease Control And Pr...

764 PUBLICATIONS 26,222 CITATIONS

[SEE PROFILE](#)

# Dynamic Characterization of Graphene Growth and Etching by Oxygen on Ru(0001) by Photoemission Electron Microscopy

Yi Cui, Qiang Fu,\* Hui Zhang, Dali Tan, and Xinhe Bao\*

State Key Laboratory of Catalysis, Dalian Institute of Chemical Physics, the Chinese Academy of Sciences, Dalian 116023, People's Republic of China

Received: May 20, 2009; Revised Manuscript Received: October 15, 2009

Epitaxial growth of graphene on Ru(0001) was investigated by photoemission electron microscopy (PEEM) and scanning tunneling microscopy (STM). By connecting the mesoscopic length scale of PEEM and the microscopic length scale of STM, we show that graphene overlayers with sizes ranging from nanometers to sub-millimeters have been prepared on Ru(0001) in a well-controllable fashion. From the systematic investigation of different methods to grow graphene on Ru(0001), the dominant factors in the graphene growth process have been revealed, which enables to grow graphene on transition metal surfaces in a controllable way. Additionally, the dynamic process of graphene etching by oxygen at temperatures between 600–1000 K was studied by *in situ* PEEM. The reaction kinetics results show that decrease in the graphene overlayers size is linearly dependent on the reaction time, indicating a reaction-controlled process. The catalytic effect of Ru substrate facilitates graphene oxidation, which shows relatively low activation energy of 27.2 kJ/mol.

## 1. Introduction

Carbon overlayers on transition metal surfaces have been attracting long-standing attention because of their relevance to catalyst deactivation in many catalytic reactions.<sup>1,2</sup> The formation of carbon on metal catalysts, so-called coke formation, has to be avoided in most cases. Recently, renewed interest in metal-supported carbon has been stimulated by the discovery of graphene, a two-dimensional (2D) carbon atomic crystal.<sup>3,4</sup> Epitaxial growth on transition metal surfaces represents one important route for producing the 2D carbon material, and much efforts have been devoted to this aspect.<sup>5</sup>

Graphene overlayers have been grown on various metal surfaces, such as Pt(111),<sup>2,6–9</sup> Ni(111),<sup>10–16</sup> Ir(111),<sup>17–24</sup> and Ru(0001).<sup>24–33</sup> Through surface segregation from metal bulk or deposition from external carbon sources, supported graphene can be produced in sizes ranging from the nanoregime<sup>23,32</sup> to macro-scale films of millimeter<sup>33</sup> and even centimeter size.<sup>34,35</sup> The graphene overlayers produced by vapor deposition are often monolayers because of the self-limiting growth of graphene on metals. Nevertheless, bilayer or few-layer graphene structures have also been successfully grown on Ru<sup>29,31</sup> and Ni<sup>34,35</sup> surfaces using the surface segregation technique. More importantly, the electronic structure of graphene can be modulated via intercalation of inert metal atoms<sup>11–16,18</sup> or oxygen atoms<sup>32</sup> at the graphene/metal interfaces or by forming multilayer structures such that the supported graphene overlayers may retain the intrinsic electronic properties of freestanding graphene. These previous results indicate that epitaxial growth of graphene on metals shows itself as a promising method to the simple and reliable fabrication of graphene layers. It has been demonstrated that the epitaxially grown graphene structures were strongly affected by many factors, such as the metal substrate, carbon flux, and growth temperature.<sup>5,24,25</sup> Understanding of the fundamental processes of graphene formation on metals is critical

for producing graphene with controlled dimension, thickness, and electronic structures.

Besides the growth of graphene, the stability of graphene is of great importance in many cases, in particular in gaseous environments. Graphene may be used as a highly sensitive gas detector,<sup>36</sup> a passivation layer against reactive environments,<sup>15</sup> and a hydrogen storage material.<sup>37</sup> The interaction of gases, such as H<sub>2</sub>, O<sub>2</sub>, H<sub>2</sub>O, CO, NO, NH<sub>3</sub>, and NO<sub>2</sub>, with graphene is important to these applications. Moreover, reaction of graphene with oxygen-, hydrogen-, and nitrogen-containing molecules could result in surface functionalization of graphene, which produce graphene oxide, graphane, and nitrogen-doped graphene, respectively.<sup>38–42</sup> Therefore, the surface chemistry of graphene needs to be explored in detail.

Scanning tunneling microscopy (STM) and low-energy electron microscopy (LEEM) are the most frequently used imaging techniques to study graphene growth. Photoemission electron microscopy (PEEM) is also a dedicated surface imaging technique, which has been often applied to investigate surface dynamic processes, such as surface reactions<sup>43</sup> and surface film growth.<sup>44</sup> With the capability of real-time dynamic imaging at micrometer scale, PEEM may be an ideal tool to investigate the growth and surface reaction of graphene overlayers supported on metals.

In the present work, graphene growth on Ru(0001) was attempted through different preparation routes. A combined STM and PEEM investigation of graphene growth on Ru(0001) has established an effective method for studying graphene growth on metals, which allow us to determine the dominant factors in the graphene growth on metals. Furthermore, the stability of graphene on Ru(0001) in O<sub>2</sub> was *in situ* investigated by using PEEM. It was shown that graphene islands can be preferably etched from the edges by oxygen and the etching process is reaction-controlled. The activation energy of the oxidation reaction was determined to be 27.2 kJ/mol.

\* To whom correspondence should be addressed. Phone: +86-411-84686637. Fax: +86-411-84694447. E-mail: xhba@dicp.ac.cn (X.B.); qfu@dicp.ac.cn (Q.F.).

## 2. Experimental Details

All experiments were carried out in a customized Omicron multichamber system, in which samples can be transferred among the preparation chamber, microscopic chamber, and spectroscopic chamber without breaking the ultrahigh vacuum (UHV) environment.<sup>32,45</sup> The microscopic chamber was equipped with STM (Omicron VT AFM) and ultraviolet-PEEM (UV-PEEM) (Focus IS-PEEM). STM was conducted in the constant current mode at room temperature (RT) using a homemade tungsten (W) tip. For PEEM imaging, the samples were irradiated by a 100-W mercury short-arc lamp with photon energy of the main UV line at about 4.9 eV. An electron beam heater was integrated into the PEEM sample stage and used to heat the samples up to 2000 K. In situ PEEM imaging can be performed in the temperature range from RT to 1100 K. If the surface needs to be heated above 1100 K, PEEM images were then recorded at RT under the same imaging conditions. Field of view (FoV) of our UV-PEEM is in the range between 6 and 500  $\mu\text{m}$ , and the image size was calibrated using a standard Si sample covered with palladium stripes. The best achieved spatial resolution of the UV-PEEM is around 30 nm.

Various gases, such as O<sub>2</sub> and C<sub>2</sub>H<sub>4</sub>, can be introduced into each chamber by directly backfilling the chambers through leak valves. The gas exposure was calculated in the unit of Langmuir (L) using the relevant gas pressure times the elapsed time (1 L = 1.3  $\times$  10<sup>-6</sup> mbar·s). The sample temperatures lower than 1100 K were measured by a chromel-alumel thermocouple, while temperatures higher than 1100 K were monitored by an infrared thermometer (Land Cyclops 100).

Clean Ru(0001) surface was prepared by cycles of Ar<sup>+</sup> sputtering (1.5 keV) and UHV annealing up to 1600 K, which produces the flat surface with straight steps. To remove any carbon impurities from the near surface region, cycles of long-time annealing in UHV at 1100 K and subsequent heating in 1.6  $\times$  10<sup>-6</sup> mbar O<sub>2</sub> at 800 K have to be carried out until that no carbon segregation happens when annealing in UHV above 1100 K.

Three different methods were employed to grow graphene on the Ru(0001) surface: (1) chemical vapor deposition (CVD), where the hot metal surface is exposed to hydrocarbon precursors;<sup>8,9,18,19,21–23</sup> (2) temperature programmed growth (TPG), in which a layer of hydrocarbons is adsorbed onto the metal surface near RT and then annealed stepwise to elevated temperatures;<sup>6,7,23,27,32,46</sup> (3) high temperature segregation (HTS), in which graphene forms on metal surfaces via surface segregation of carbon from metal bulk at high temperatures.<sup>25–27,29,33</sup>

## 3. Results and Discussion

**3.1. Growth of Graphene on Ru(0001).** Graphene growth was first attempted by CVD. The Ru(0001) surface was exposed to 3.9  $\times$  10<sup>-8</sup> mbar C<sub>2</sub>H<sub>4</sub> at 1100 K, and the growth was monitored by using PEEM. A series of snapshots from the PEEM video are shown in panels A–D of Figure 1. The clean Ru(0001) surface presents itself as dark region (Figure 1A) because the surface work function (5.4 eV) is much larger than the photon energy of the main UV line (4.9 eV). After 40 s, white dots with size smaller than 1  $\mu\text{m}$  appear in the PEEM field of view. It is frequently observed that covering transition metal surfaces by carbon overlayers significantly decreases the surface work function.<sup>47</sup> For example, the work function of a Ru(0001) surface covered by one layer of graphene was reported to decrease to 4.5<sup>48</sup> or even 3.9 eV.<sup>49</sup> The lower surface work function of the graphene-covered Ru(0001) surface should give rise to a brighter PEEM image compared to the clean Ru(0001)

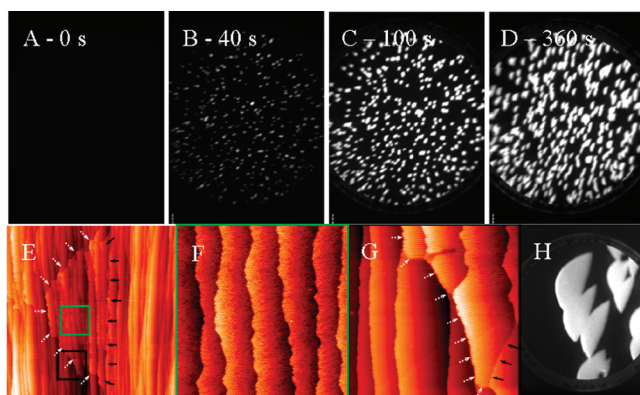


**Figure 1.** Time elapsed PEEM images (A–D, FoV = 100  $\mu\text{m}$ ) when exposing Ru(0001) to 3.9  $\times$  10<sup>-8</sup> mbar C<sub>2</sub>H<sub>4</sub> at 1100 K. Exposure times were 0, 40, 100, and 360 s for A–D, respectively. STM images (E–G) from a graphene/Ru(0001) surface corresponding to that shown in part C: 1200 nm  $\times$  1200 nm in (E) and 200 nm  $\times$  200 nm in (F) and (G). (H): PEEM image (FoV = 300  $\mu\text{m}$ ) from Ru(0001) exposed to 3.9  $\times$  10<sup>-8</sup> mbar C<sub>2</sub>H<sub>4</sub> for 600 s at 1200 K.

surface. Therefore, we interpreted the white dots in the PEEM images to be graphene islands formed on Ru(0001). The series of PEEM images shown in Figure 1 demonstrated that all the graphene islands keep on growing but the number of nucleation sites almost remains constant with the increasing exposure time. After exposure for 360 s most of the graphene islands are larger than 5  $\mu\text{m}$  and some islands even connect to each other (Figure 1D). More interestingly, sector shape can be discerned in many graphene islands.

STM was used to investigate the Ru(0001) surface exposed to 3.9  $\times$  10<sup>-8</sup> C<sub>2</sub>H<sub>4</sub> at 1100 K for 100 s (Figure 1, panels E–G), which correspond to the surface shown in Figure 1C. After the exposure, the surface was kept at 1100 K for 3 min to get to an equilibrium surface state at this temperature,<sup>28</sup> and then cooled down to RT for STM studies. Figure 1E shows a typical surface topography at large scale, where an individual graphene island with monolayer thickness can be seen. As indicated by the short arrows, the island presents a trianglelike shape, which is similar to what we have observed in PEEM images (Figure 1C). The island surface structure was further illustrated in Figure 1F. Typical moiré patterns due to superposition of the monolayer graphite lattice on the Ru(0001) lattice can be clearly resolved.<sup>26,27,32,33</sup> However, some defects can be seen on the surface, which may be due to the relatively low growth temperature. Figure 1G displays the surface morphology at the island edge, which shows two kinds of boundaries between the clean Ru(0001) and the graphene domain. The white arrows (dashed lines) indicate the unsaturated graphene edges while the black arrows (solid lines) point to the edges saturated by the upper Ru(0001) steps. The STM data are consistent with the PEEM results, confirming the formation of micrometer-sized monolayer graphene islands on Ru(00001) by CVD.

Alternatively, graphene growth was attempted by the TPG method. A total of 3 L of C<sub>2</sub>H<sub>4</sub> was adsorbed on the clean Ru(0001) at RT, and the surface was subsequently heated at a rate of 40 K min<sup>-1</sup> in UHV. The heating process between RT and 1300 K was monitored by PEEM. Parts A and B of Figure 2 display two PEEM images recorded from the surface after annealing at 900 and 1100 K, respectively. Though neither image shows any well-defined surface structures, higher gray intensity appears in comparison to the clean Ru(0001) surface (see Figure 1A). STM images recorded from the corresponding surfaces are shown in parts D and E of Figure 2, which indicate

the formation of graphene nanoislands or nanoclusters distributed evenly on the surface. The characteristic moiré patterns on the nanostructured graphene islands are apparent in the inset micrographs. The Ru(0001) surface covered by a high density of nanographene structures should have a smaller surface work function than the clean metal surface. Therefore, the surfaces present brighter, albeit blurry, PEEM images. Annealing the surface at 1300 K produces a high contrast PEEM image (Figure 2C), like the images in parts B–D of Figures 1. The bright regions are from microsized graphene islands and the dark regions represent the bare Ru(0001) surface.

The third route for the preparation of graphene is the surface segregation process. It is known that carbon can be dissolved in many transition metals at high temperatures. The lower solubility of carbon in bulk metals at decreasing temperature may drive the surface segregation of carbon. On the clean Ru(0001) surface, carbon was specially introduced into the near surface regions through cycles of saturated adsorption of hydrocarbons (e.g.,  $C_2H_4$ ) at RT and flashing to 1600 K. Since the sample was cooled down quickly the topmost surface is clean from any carbon flakes as confirmed by STM and PEEM. However, a substantial amount of carbon has been dissolved at the subsurface region or into the Ru(0001) bulk. The resulting “clean” Ru(0001) surface was subjected to the high temperature segregation (HTS), which was studied *in situ* by PEEM. Parts A–D of Figures 3 show a time-elapsed process when keeping the sample at 1100 K. It can be seen that graphene islands appeared on the surface rapidly and continued to grow in the lateral direction during the annealing process. To see the process in more detail, we chose one island to follow its evolution as a function of segregation time, shown in the inset micrographs. As marked by the arrows in Figure 3A, the island grows in three lateral directions and a sector-shaped graphene island with a size ca.  $10\ \mu m$  forms after HTS for 900 s. Increasing the annealing temperature in the surface segregation experiment results in quite a different morphology. For example, a “clean” surface was heated at 1260 K for 20 min, the surface morphology of which is given in Figure 3E. In comparison to the images

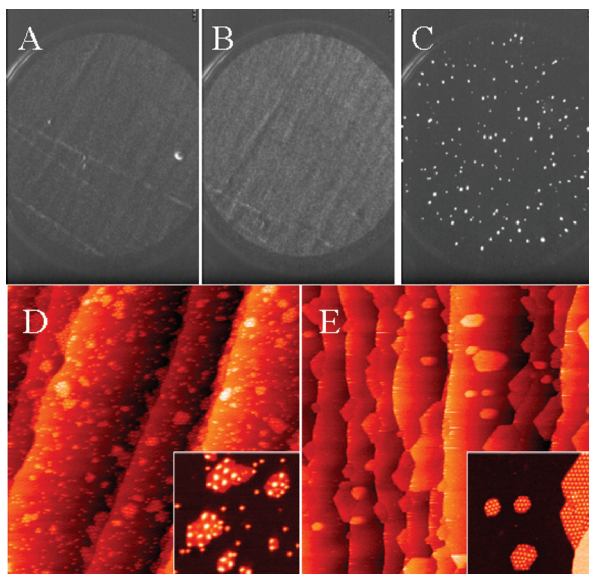


**Figure 2.** PEEM (A, B, and C, FoV =  $120\ \mu m$ ) and STM images (D and E) from the Ru(0001) surface preadsorbed by 3 L  $C_2H_4$  at RT followed by annealing at 900 K (A and D), 1100 K (B and E), and 1300 K (C) in UHV, respectively.  $200\ nm \times 200\ nm$  (D) and  $40\ nm \times 40\ nm$  for the inset;  $400\ nm \times 400\ nm$  (E) and  $100\ nm \times 100\ nm$  for the inset.

shown in parts A–D of Figures 3, this PEEM image presents homogeneous contrast and high brightness in the field of view, which indicates the formation of graphene with high coverage and high dispersion. Compared to the limited graphene island density in the case of HTS at 1100 K, it seems that at 1260 K more surface sites are available for outward diffusion of carbon from the Ru(0001) bulk, and thus more graphene islands can nucleate and grow simultaneously.

**3.2. Etching by Oxygen of Graphene on Ru(0001).** It has been reported that graphene can be used as a protective layer to prevent metal surfaces from oxidizing near RT.<sup>15,30,32</sup> However, stability of the graphene in gaseous atmosphere at elevated temperatures remains less explored. Here, *in situ* PEEM was employed to study the stability of the Ru(0001) supported graphene in  $O_2$ . Graphene/Ru(0001) samples were prepared by HTS at 1100 K as those shown in parts A–D of Figures 3. The surfaces were annealed in  $1.3 \times 10^{-6}\ mbar\ O_2$  at different temperatures. *In situ* PEEM imaging was carried out isothermally. Below 600 K no obvious changes were observed by PEEM, but oxygen intercalation is known to occur as revealed by STM.<sup>32</sup> The graphene islands start to shrink when heating the surface at 600 K. Parts A–D of Figure 4 display four snapshots of the PEEM video recorded from the surface exposed to  $1.3 \times 10^{-6}\ mbar\ O_2$  at 600 K. All the graphene islands continue to decrease in size with the annealing time and have completely vanished from the surface after 800 s. The red lines highlight the profile of the original island before oxidation and the island evolution with annealing time indicates that the island shrinks inward. The situation is just opposite to the case of graphene growth in the HTS process, in which graphene islands expand outward (Figure 3). To evaluate the evolution of graphene islands with oxidation in more detail, the dimensions of the island (the highlighted one in Figure 4) parallel to the Ru(0001) step and perpendicular to the step were quantitatively derived from the PEEM video and plotted against the oxidation time (Figure 5). For comparison, both dimensions of the growing island (the inset of Figure 3) are included. Except for the initial periods, the ratio of the island dimension along the step to that perpendicular to the step remains almost constant, approximately 2.

Furthermore, the  $O_2$  etching reaction data displayed in Figure 5 show that the etching of graphene shows linear dependence on reaction time, which suggests that the etching process is controlled by the oxidation. To derive the reaction kinetic data, oxidation has been performed at different temperatures. *In situ* PEEM investigation of graphene islands etched by oxygen was carried out at reaction temperatures from 600 to 1000 K, leaving the oxygen partial pressure constant at  $1.3 \times 10^{-6}\ mbar$ . The dimensions of the graphene islands parallel to Ru(0001) steps were plotted as a function of the oxidation time, as shown in Figure 6. In the temperature range we studied, the graphene etching rate was almost constant at each temperature point. Ignoring the temperature effect to the activation energy of the reaction, we calculated the total reaction activation energy of graphene etching by  $O_2$  on the Ru(0001) surface to be  $27.2\ kJ/mol$  according to the Arrhenius plot (see inset of Figure 6). This value is lower than that from the typical carbon oxidation reactions, such as carbon combustion<sup>50</sup> or graphite oxidation.<sup>51</sup> Since the Ru(0001) surface shows strong ability to dissociatively adsorb  $O_2$ ,<sup>52</sup> the catalytic dissociation of  $O_2$  into atomic oxygen species via the metal substrate may facilitate carbon oxidation in  $O_2$ , similar to the finding for the promotion effect of Ca addition to oxidation of microporous carbon.<sup>53</sup>

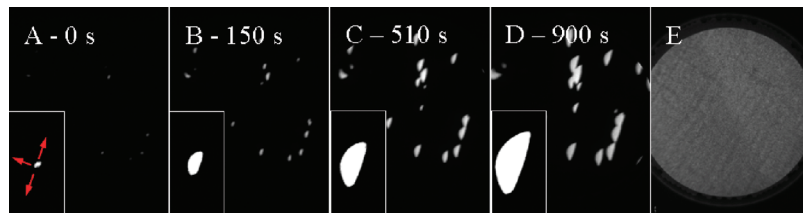


**Figure 3.** Time elapsed PEEM images (A–D, FoV = 100  $\mu\text{m}$ ) recorded in situ from a “clean” Ru(0001) surface annealed at 1100 K in UHV. The time interval was 150, 510, and 900 s, respectively. The inset graphs (bottom left of parts A–D) show the process of a typical island growth during the high temperature surface segregation. (E) Static PEEM image recorded from the Ru(0001) at RT after annealing a “clean” Ru(0001) at 1260 K for 20 min (FoV = 120  $\mu\text{m}$ ).

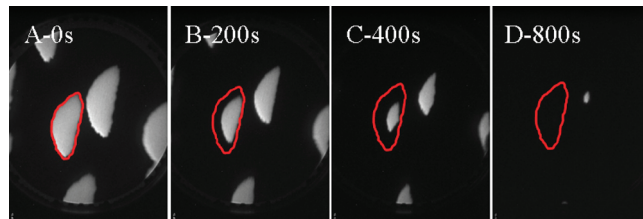


**Figure 4.** Time-elapsed PEEM images (A–D, FoV = 100  $\mu\text{m}$ ) recorded in situ from a graphene covered Ru(0001) surface heated in  $1.3 \times 10^{-6}$  mbar  $\text{O}_2$  at 600 K. The time interval was 200, 400, and 800 s, respectively. The red lines highlight the profile of the original island before oxidation.

### 3.3. Growth and Etching Mechanism of Graphene on Ru(0001).

In the present work, we have made a systematic study of graphene growth and  $\text{O}_2$  etching on Ru(0001) by using PEEM. On the basis of dynamic characterization with PEEM and high resolution surface imaging by STM, some dominant factors in growth and stability of graphene can be derived as follows.

First, the results reveal that graphene can be epitaxially grown on Ru(0001) irrespective of the origin of the carbon source which can be supplied by decomposition of gaseous hydrocarbons in the CVD and TPG processes or through outward diffusion of interstitial carbon from metal bulk in the HTS method. For TPG, the graphene coverage is limited by the saturation adsorption amount of hydrocarbons on metals at RT. For example, only 0.25 ML graphene was produced in the case of saturated adsorption of  $\text{C}_2\text{H}_4$  on Pt(111) and Ru(0001) at RT.<sup>2,7,32</sup> Repeating the TPG process several times increased the graphene coverage up to nearly 1 ML.<sup>46</sup> The amount of surface graphene obtained by CVD is simply controlled by exposure of hydrocarbons. With enough exposure of hydrocarbons to the surface, graphene could cover the whole surface. In the HTS process, the surface segregated carbon is limited by carbon dissolved in the bulk of the metals. With enough carbon at the near surface region, which could be supplied by depositing carbon, graphene islands would grow in size until they contact each other and form large islands with sizes on the order of several hundreds of micrometers.<sup>29</sup> Therefore, graphene coverage can be controlled by the amount of carbon species available to the surface in all the preparation processes.

Second, the temperature is another important parameter to influence the structure and morphology of the grown graphene overlayers. In the TPG process, stepwise annealing of the surface preadsorbed by 3 L of  $\text{C}_2\text{H}_4$  at RT leads to formation of carbon species on the surface around 700 K.<sup>32</sup> At the low temperatures ( $\leq 1100$  K), the carbon species with limited surface mobility tend to aggregate at the nearest nucleation sites and form graphene nanoclusters or nanoislands there. Thus, the TPG method produces graphene islands with small size but high density (Figure 2). Only at high temperatures, for example,

1300 K (see Figure 2C), could the highly dispersed graphene nanoislands be mobile and aggregate to form micrometer-scale graphene islands, which may happen via the Smoluchowski ripening process like graphene growth on Ir(111).<sup>23</sup> In the CVD process, exposing the same amount (3 L) of  $\text{C}_2\text{H}_4$  to Ru(0001) at 1100 K already produced micrometer-sized graphene islands (Figure 1C). At this temperature, the dissociated surface carbon species could diffuse on the surface and aggregate to the far available nucleation sites. Thus, low density and micrometer-sized graphene islands form at this temperature. At even higher growth temperatures, e.g., 1200 K, submillimeter sized graphene islands could be produced on the surface (as shown in Figure 1H).

In the TPG and CVD methods, we see that higher dispersion of graphene islands was observed at lower temperature. In contrast, the temperature effect has been reversed in the HTS process, in which lower island dispersion was observed at lower temperatures (Figures 3D and 3E). The interdiffusion of carbon at the Ru(0001) surface is a thermally activated process, which may become less energy demanding at surface defect sites. Therefore, at low temperature, e.g., 1100 K, carbon mainly diffuses outward at the surface defect sites and nucleates there to form islands with limited density. However, higher temperatures could facilitate outward diffusion of carbon at more surface sites such that high density islands may nucleate and grow simultaneously on the surface, as confirmed by the result in Figure 3E. The above results suggest that the growth temperature could be used to manipulate the graphene island density and dispersion.

Finally, graphene overlayers show preferential growth and removal along certain orientations. The previous STM results and our present experimental data (Figures 1 and 2) have shown that most graphene islands prefer to nucleate at Ru(0001) surface steps.<sup>6,23,26,32</sup> One edge of the graphene sheet should be saturated by Ru atoms at the steps. When additional carbon species approach the island, they tend to incorporate into the outer edges with unsaturated C atoms. Thus, the islands expand laterally on the surface along the steps and across the steps in the downhill direction as marked in Figure 3. The increase in the observed macroscopic size of the graphene islands parallel to the steps should be roughly 2 times that perpendicular to the steps in the growth process (Figure 5). Similarly, the edges with unsaturated C atoms should present higher reactivity to gases, such as  $\text{O}_2$ , than the edge with saturated C atoms (marked by solid line arrows in Figure 1). Indeed, we observed that the islands shrink parallel to substrate steps and across the steps in the uphill direction via preferential etching of the edge carbon atoms by oxygen (Figure 4). Thus, the similar ratio around 2 between the decrease in the dimension parallel to steps and that perpendicular to the steps was also observed in the removal of

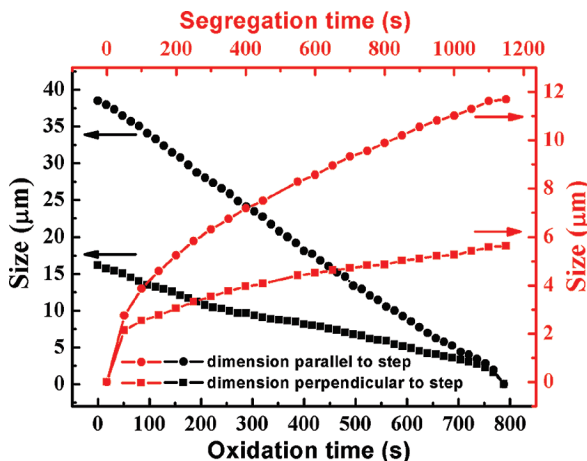


**Figure 5.** Evolution of dimensions of the islands parallel to the step and perpendicular to the step (shown in the insets of Figures 3 and 4) as a function of the segregation time and oxidation time.

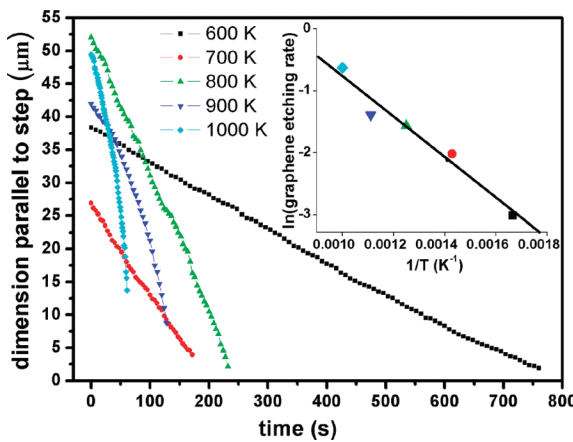


**Figure 6.** Evolution of dimensions of the islands parallel to the step at different temperatures from 600 to 1000 K at  $1.3 \times 10^{-6}$  mbar O<sub>2</sub> as a function of the oxidation time. The inset shows the graphene etching rate as a function of oxidation temperature. The solid line is fit to the Arrhenius equation.

graphene by O<sub>2</sub> (Figure 5). The preferential growth or removal of graphene could be used to control the shape of graphene islands.

#### 4. Conclusion

Growth of graphene on Ru(0001) was studied systematically by utilizing both the dynamic characterization of PEEM and the high spatial resolution capability of STM. Through the comparative study of three routes to grow graphene, namely, TPG, CVD, and HTS, the growth parameters including the carbon source and growth temperature have been identified as the critical factors in graphene formation. Furthermore, in situ PEEM was used to investigate the etching of graphene by oxygen. The removal of graphene was found to be reaction controlled, in which the decrease in the graphene overlayer size is linearly dependent on the reaction time. The activation energy of graphene etching reaction by oxygen was deduced to be 27.2 kJ/mol based on the oxidation experiments at temperatures ranged from 600 to 1000 K. Both the growth and the removal of graphene islands happen at the two directions parallel to the substrate steps and one direction perpendicular to the steps. On the basis of the understanding of growth and etching mechanism, coverage, size, dispersion, and morphology of

graphene islands may be controlled by the amount of surface carbon source, growth temperature, and substrate surface orientation.

**Acknowledgment.** This work was financially supported by the National Natural Science Foundation of China (Nos. 20603037, 20733008, and 20873143), Ministry of Science and Technology of China, and Chinese Academy of Sciences ("Bairen" program).

#### References and Notes

- Bengaard, H. S.; Noskov, J. K.; Sehested, J.; Clausen, B. S.; Nielsen, L. P.; Molenbroek, A. M.; Rostrup-Nielsen, J. R. *J. Catal.* **2002**, *209*, 365.
- Land, T. A.; Michely, T.; Behm, R. J.; Hemminger, J. C.; Comsa, G. *Surf. Sci.* **1992**, *264*, 261.
- Novoselov, K. S.; Geim, A. K.; Morozov, S. V.; Jiang, D.; Zhang, Y.; Dubonos, S. V.; Grigorieva, I. V.; Firsov, A. A. *Science* **2004**, *306*, 666.
- Geim, A. K.; Novoselov, K. S. *Nat. Mater.* **2007**, *6*, 183.
- Wintterlin, J.; Bocquet, M. L. *Surf. Sci.* **2009**, *603*, 1841.
- Land, T. A.; Michely, T.; Behm, R. J.; Hemminger, J. C.; Comsa, G. *Appl. Phys. A: Mater. Sci. Process.* **1991**, *53*, 414.
- Land, T. A.; Michely, T.; Behm, R. J.; Hemminger, J. C.; Comsa, G. *J. Chem. Phys.* **1992**, *97*, 6774.
- Ueta, H.; Saida, M.; Nakai, C.; Yamada, Y.; Sasaki, M.; Yamamoto, S. *Surf. Sci.* **2004**, *560*, 183.
- Starr, D. E.; Pazhetnov, E. M.; Stadnichenko, A. I.; Boronin, A. I.; Shaikhutdinov, S. K. *Surf. Sci.* **2006**, *600*, 2688.
- Gamo, Y.; Nagashima, A.; Wakabayashi, M.; Terai, M.; Oshima, C. *Surf. Sci.* **1997**, *374*, 61.
- Farias, D.; Shikin, A. M.; Rieder, K. H.; Dedkov, Y. S. *J. J. Phys.: Condens. Matter* **1999**, *11*, 8453.
- Shikin, A. M.; Prudnikova, G. V.; Adamchuk, V. K.; Moresco, F.; Rieder, K. H. *Phys. Rev. B* **2000**, *62*, 13202.
- Dedkov, Y. S.; Shikin, A. M.; Adamchuk, V. K.; Molodtsov, S. L.; Laubschat, C.; Bauer, A.; Kaindl, G. *Phys. Rev. B* **2001**, *64*, 035405.
- Starodubov, A. G.; Medvetskii, M. A.; Shikin, A. M.; Adamchuk, V. K. *Phys. Solid State* **2004**, *46*, 1340.
- Dedkov, Y. S.; Fonin, M.; Rudiger, U.; Laubschat, C. *Appl. Phys. Lett.* **2008**, *93*, 022509.
- Varykhalov, A.; Sanchez-Barrera, J.; Shikin, A. M.; Biswas, C.; Vescovo, E.; Rybkin, A.; Marchenko, D.; Rader, O. *Phys. Rev. Lett.* **2008**, *101*, 157601.
- Rutkov, E. V.; Tontegode, A. Y. *Surf. Sci.* **1985**, *161*, 373.
- Gall, N. R.; Rutkov, E. V.; Tontegode, A. Y. *Carbon* **2000**, *38*, 663.
- Klusek, Z.; Kozlowski, W.; Waqar, Z.; Datta, S.; Burnell-Gray, J. S.; Makarenko, I. V.; Gall, N. R.; Rutkov, E. V.; Tontegode, A. Y.; Titkov, A. N. *Appl. Surf. Sci.* **2005**, *252*, 1221.
- N'Diaye, A. T.; Bleikamp, S.; Feibelman, P. J.; Michely, T. *Phys. Rev. Lett.* **2006**, *97*, 215501.
- Coraux, J.; N'Diaye, A. T.; Busse, C.; Michely, T. *Nano Lett.* **2008**, *8*, 565.
- N'Diaye, A. T.; Coraux, J.; Plasa, T. N.; Busse, C.; Michely, T. *New J. Phys.* **2008**, *10*, 043033.
- Coraux, J.; N'Diaye, A. T.; Engler, M.; Busse, C.; Wall, D.; Buckanie, N.; Heringdorf, F. J. M. Z.; van Gastei, R.; Poelsema, B.; Michely, T. *New J. Phys.* **2009**, *11*, 023006.
- Loginova, E.; Bartelt, N. C.; Feibelman, P. J.; McCarty, K. F. *New J. Phys.* **2009**, *11*, 063046.
- McCarty, K. F.; Feibelman, P. J.; Loginova, E.; Bartelt, N. C. *Carbon* **2009**, *47*, 1806.
- Marchini, S.; Gunther, S.; Wintterlin, J. *Phys. Rev. B* **2007**, *76*, 075429.
- de Parga, A. L. V.; Calleja, F.; Borca, B.; Passeggi, M. C. G.; Hinarejos, J. J.; Guinea, F.; Miranda, R. *Phys. Rev. Lett.* **2008**, *1*, 056807.
- Loginova, E.; Bartelt, N. C.; Feibelman, P. J.; McCarty, K. F. *New J. Phys.* **2008**, *10*, 093026.
- Sutter, P. W.; Flege, J. I.; Sutter, E. A. *Nat. Mater.* **2008**, *7*, 406.
- Borca, B.; Calleja, F.; Hinarejos, J. J.; de Parga, A. L. V.; Miranda, R. J. *J. Phys.: Condens. Matter* **2009**, *21*, 134002.
- Sutter, E.; Acharya, D. P.; Sadowski, J. T.; Sutter, P. *Appl. Phys. Lett.* **2009**, *94*, 133101.
- Zhang, H.; Fu, Q.; Cui, Y.; Tan, D.; Bao, X. *J. Phys. Chem. C* **2009**, *113*, 8296.
- Pan, Y.; Zhang, H. G.; Shi, D. X.; Sun, J. T.; Du, S. X.; Liu, F.; Gao, H. *J. Adv. Mater.* **2009**, *21*, 2777.
- Kim, K. S.; Zhao, Y.; Jang, H.; Lee, S. Y.; Kim, J. M.; Kim, K. S.; Ahn, J.-H.; Kim, P.; Choi, J.-Y.; Hong, B. H. *Nature* **2009**, *457*, 706.

- (35) Reina, A.; Jia, X.; Ho, J.; Nezich, D.; Son, H.; Bulovic, V.; Dresselhaus, M. S.; Kong, J. *Nano Lett.* **2009**, *9*, 30.
- (36) Schedin, F.; Geim, A. K.; Morozov, S. V.; Hill, E. W.; Blake, P.; Katsnelson, M. I.; Novoselov, K. S. *Nat. Mater.* **2007**, *6*, 652.
- (37) Patchkovskii, S.; Tse, J. S.; Yurchenko, S. N.; Zhechkov, L.; Heine, T.; Seifert, G. *Proc. Natl. Acad. Sci. U.S.A.* **2005**, *102*, 10439.
- (38) Wei, D. C.; Liu, Y. Q.; Wang, Y.; Zhang, H. L.; Huang, L. P.; Yu, G. *Nano Lett.* **2009**, *9*, 1752.
- (39) Wang, X. R.; Li, X. L.; Zhang, L.; Yoon, Y.; Weber, P. K.; Wang, H. L.; Guo, J.; Dai, H. J. *Science* **2009**, *324*, 768.
- (40) Elias, D. C.; Nair, R. R.; Mohiuddin, T. M. G.; Morozov, S. V.; Blake, P.; Halsall, M. P.; Ferrari, A. C.; Boukhalov, D. W.; Katsnelson, M. I.; Geim, A. K.; Novoselov, K. S. *Science* **2009**, *323*, 610.
- (41) Li, D.; Muller, M. B.; Gilje, S.; Kaner, R. B.; Wallace, G. G. *Nanotech.* **2008**, *3*, 101.
- (42) Jeong, H. K.; Lee, Y. P.; Lahaye, R.; Park, M. H.; An, K. H.; Kim, I. J.; Yang, C. W.; Park, C. Y.; Ruoff, R. S.; Lee, Y. H. *J. Am. Chem. Soc.* **2008**, *130*, 1362.
- (43) Kim, M.; Bertram, M.; Pollmann, M.; Oertzen, A. v.; Mikhailov, A. S.; Rotermund, H. H.; Ertl, G. *Science* **2001**, *292*, 1357.
- (44) Meyer zu Heringdorf, F.-J.; Reuter, M. C.; Tromp, R. M. *Nature* **2001**, *412*, 517.
- (45) Zhang, H.; Fu, Q.; Yao, Y. X.; Zhang, Z.; Ma, T.; Tan, D. L.; Bao, X. H. *Langmuir* **2008**, *24*, 10874.
- (46) Zhang, H.; Fu, Q.; Cui, Y.; Tan, D.; Bao, X. *Chin. Sci. Bull.* **2009**, *54*, 2446.
- (47) Oshima, C.; Nagashima, A. *J. J. Phys.: Condens. Matter* **1997**, *9*, 1.
- (48) Himpel, F. J.; Christmann, K.; Heimann, P.; Eastman, D. E.; Feibelman, P. J. *Surf. Sci.* **1982**, *115*, L159.
- (49) Brugger, T.; Gunther, S.; Wang, B.; Dil, J. H.; Bocquet, M.-L.; Osterwalder, J.; Wintterlin, J.; Greber, T. *Phys. Rev. B* **2009**, *79*, 045407.
- (50) Du, Z. Y.; Sarofim, A. F.; Longwell, J. P.; Mims, C. A. *Energy Fuels* **1991**, *5*, 214.
- (51) Hahn, J. R.; Kang, H.; Lee, S. M.; Lee, Y. H. *J. Phys. Chem. B* **1999**, *103*, 9944.
- (52) Wheeler, M. C.; Seets, D. C.; Mullins, C. B. *J. Chem. Phys.* **1996**, *105*, 1572.
- (53) Floess, J. K.; Longwell, J. P.; Sarofim, A. F. *Energy Fuels* **1988**, *2*, 756.

JP907949A